 doi:10.20944/preprints201808.0246.v2

Article

A Hybrid Lagrangian-Eulerian Particle Model for Ecosystem Simulation

Pengfei Xue [1,2*], David J Schwab [3], Xing Zhou [1], Chenfu Huang [1], Ryan Kibler [1], Xinyu Ye [1]

[1] Department of Civil and Environmental Engineering, Michigan Technological University, Houghton, Michigan
[2] Great Lakes Research Center, Michigan Technological University, Houghton, Michigan
[3] Michigan Tech Research Institute, Michigan Technological University, Ann Arbor, Michigan
* Corresponding author: Dr. Pengfei Xue, Michigan Tech, 1400 Townsend Dr., Building GLRC-317, Houghton, MI 49931; E-mail: pexue@mtu.edu

Abstract: Current numerical methods for simulating biophysical processes in aquatic environments are typically constructed in a grid-based Eulerian framework using the advection-diffusion equation for physical transport with source and sink terms describing biological processes. Often, the biogeochemical processes and physical (hydrodynamic) processes occur at different time and space scales, and changes in biological processes do not affect the hydrodynamic conditions. Therefore, it is possible to develop an alternative strategy to grid-based approaches for linking hydrodynamic and biogeochemical models that can significantly improve computational efficiency for this type of linked biophysical model. In this work, we utilize a new technique which links hydrodynamic effects and biological processes through a property-carrying particle model (PCPM) in a Lagrangian/Eulerian framework. The model is tested in idealized cases and its utility is demonstrated in a practical application to Sandusky Bay. Results show the integration of Lagrangian and Eulerian approaches allows for a natural coupling of mass transport (represented by particle movements and random walk) and biological processes in water columns which is described by a nutrient-phytoplankton-zooplankton-detritus (NPZD) biological model. This method is far more efficient than traditional tracer based Eulerian biophysical models for 3-D simulation, particularly for a large domain and/or ensemble simulations.

Keywords: Property-carrying Particle Model; Ecosystem Simulation; Biophysical Modeling; Sandusky Bay; Great Lakes

1. Introduction

Current numerical methods for simulating biogeochemical processes in aquatic environments are typically constructed in a grid-based Eulerian framework. Equations for the time evolution of state variables of the biophysical model include advection and diffusion terms which depend on hydrodynamic variables, as well as source and sink terms representing growth, decay, and interaction with other biogeochemical variables. The property concentration fields ($C_i, i = 1,2,3$ ....) are often calculated using a set of advection-diffusion equations:

$$\frac{\partial DC_i}{\partial t} + \frac{\partial DuC_i}{\partial x} + \frac{\partial DvC_i}{\partial y} + \frac{\partial DwC_i}{\partial z} - \frac{1}{D}\frac{\partial}{\partial z}\left(K_h \frac{\partial C_i}{\partial z}\right) - DF_c = C_{i,source} - C_{i,sink} \quad (1)$$

where D is the total water depth, u, v, and w are the x, y, and z components of the water velocity, K_h is the vertical thermal diffusion coefficient, F_c is the horizontal diffusion term, and $C_{i,source}$ and $C_{i,sink}$ represents the sources and sinks of C_i, respectively, due to the biological processes which are typically described using a set of biological process equations. This approach has been widely used in coastal and ocean modeling communities [e.g. 1-4].

A major practical challenge is that the biological submodel often involves a large group of parameters for calibration and confirmation which requires a considerable amount of computational time to tune the model. As shown in Equation 1, tuning the simulation of biological processes (e.g. changes in parameterization, initial and boundary conditions) requires a complete time integration

 doi:10.20944/preprints201808.0246.v2

of the entire equation so that the impact of physical process (advection and diffusion) on the biological properties can be properly incorporated. However, the biophysical process is generally not two-way coupled. In other words, one can often assume that changes in biological processes (in our case, the resulting changes in NPZD property concentration) do not affect the hydrodynamic condition (currents, temperature, mixing, etc.). This indicates that there may be a more computationally efficient approach to resolve the impact of hydrodynamics on the biological processes rather than directly integrate Equation 1 every time the biological submodel is tuned.

The PCPM is developed to test the feasibility of an alternative strategy to grid-based approaches for linking hydrodynamic and biogeochemical models that may reduce the problems mentioned above. Instead of grid-based, time-averaging of hydrodynamic variables, the hydrodynamic model is used to calculate the Lagrangian trajectories of a large number of current-following tracer particles; these trajectories become the linking mechanism between the hydrodynamic model and the biogeochemical model. In hybrid Lagrangian-Eulerian PCPM, each current-following tracer particle carries with it a number of time-varying properties which correspond to the state variables of the biogeochemical model. The PCPM also employs its own horizontal grid system or series of regions which is independent of the hydrodynamic model grid and is used to calculate local average values of the particle-based properties. These cell-based properties allow all particles within a PCPM cell to influence the properties of other particles within the same cell or region and allow for display and analysis of biogeochemical fields.

The remaining sections of this paper are organized as follows: Details of PCPM are described in section 2. The results and discussion of two idealized experiments are presented in section 3. The application of PCPM to Sandusky Bay is presented in section 4. A discussion and summary of the PCPM is concluded in section 5.

2. Methods

In this implementation of PCPM, particle trajectories are pre-computed based on the output of a hydrodynamic model and are independent of the particle properties. An initial particle density (i.e., total number of particles / volume of computational domain) is selected and particles are randomly distributed throughout the computational domain. Particles are not allowed to leave the computational domain except at hydrodynamic outflows. At hydrodynamic inflows, new particles are introduced with the same density as the initial distribution. The total number of active particles is not strictly preserved, but if there is a net balance of hydrodynamic inflows and outflows, the total number of particles is approximately constant.

An alternative approach to implementing a PCPM would allow particle-based properties to influence particle trajectories, perhaps through buoyancy or sinking. In this case, the PCPM would have to be directly coupled with the particle trajectory calculation. In the initial implementation of PCPM this paper, we consider only the uncoupled case.

Any suitable method can be used to generate the Lagrangian particle trajectories. Typically, the trajectories are calculated from a time integration of the Lagrangian equations of motion:

$$\frac{dx}{dt} = u, \frac{dy}{dt} = v, \frac{dz}{dt} = w \quad (2)$$

where (x,y,z) is the particle's position in 3 dimensions, (u,v,w) is the local fluid velocity vector, and t is time. For the two idealized examples presented in this paper, the trajectories are calculated semi-analytically from a simple, idealized flow field. The third, more realistic example, demonstrates the use of a full hydrodynamic model of a natural basin (i.e., Sandusky Bay) to compute currents and trajectories.

PCPM uses a computational grid system which is independent of the grid system used to compute currents for particle trajectories. The PCPM computational cells are used to define regions in which the properties carried by the particles are allowed to interact with one another. In this respect, PCPM is similar to the classic Particle-in-Cell (PIC) method with PM (particle-mesh) interactions. PIC methods can also be mesh-independent by allowing direct particle-particle (PP) interactions, or a combination of PM and PP [5-8]. In PCPM, a basic simplifying assumption is that

Preprints (www.preprints.org) | NOT PEER-REVIEWED | Posted: 17 August 2018 doi:10.20944/preprints201808.0246.v2

only particles within a single PCPM cell are allowed to interact, such as the PIC PM method. The advantage of this approach is that it is conceptually intuitive to implement and computationally efficient to program.

Each computational time step in the PCPM consists of six intermediate steps:

1. Read particle locations (x, y, z) and temperature at this location for all tracer particles at this time step. Locations are pre-computed based on currents from a hydrodynamic model.
2. Determine the PCPM cell for each particle. Cells can be 2-D or 3-D.
3. Apply boundary conditions to any particle-based properties that require them.
4. Calculate PCPM cell-based average of each property.
5. Calculate the time evolution of the cell-based properties (and particle-based properties, if necessary) using the process equations defined for that property.
6. Redistribute cell-based properties to particles within each cell by replacing the particle-based property with a weighted average of the particle-based property and the new cell-based property.

Note that all steps except 3 and 5 are independent of the specific problem, i.e., they will be carried out the same way no matter how many properties are attached to the particles or what those properties represent. More importantly, steps 1 and 2 only need to be run once regardless of modifications in biological processes at the later stage. These are two of the key designs of PCPM for the enhanced computational efficiency.

Consider each of these steps in detail:

1. Read particle locations (x, y, z) and temperature. This step simply updates the location of each particle that is being used in the computation. Figure 1 is a conceptual representation of a PCPM computational cell, Particles (m_1, m_2, m_3, …) move in and out of the cell at each PCPM time step based on their trajectories as computed from the hydrodynamic model. The total number of particles for a particular computation is assumed to be fixed for the duration of the computation, although some particles may enter or leave the PCPM domain during the computation. Water temperature or other physical properties from the hydrodynamic calculation can be stored along with the pre-computed particle trajectories and can be included as one of the properties (*P1, P2, P3*, …) carried by the particle.
2. Determine the PCPM cell for each particle. In Figure 1, the PCPM cell is represented by the enclosing rectangle. The PCPM domain need not coincide with the domain that was used for the hydrodynamic simulation and computation of particle trajectories. It can be regular or irregular, as long as there is a prescribed method to calculate which PCPM cell contains a prescribed particle position (x, y, z). The PCPM cells are the volumes within which particle properties can interact, that is, during a single time step, all particles within a PCPM cell can influence the evolution of particle properties within that cell, but are independent of other cells.
3. Apply boundary conditions to any particle-based properties that require them. If there is a property (e.g., concentration of a dissolved nutrient) that needs to be specified as a boundary condition, then particles within the cell where the boundary condition needs to be applied will have that property adjusted to meet the boundary condition. For example, in a cell that is associated with an inflow to the domain, the properties that are being carried into the domain through the inflow are adjusted to take account of the change in that property for particles within that cell. Alternatively, if particles from the hydrodynamic-based trajectory calculation are entering a PCPM cell, the values of the associated properties for each particle need to be specified.
4. Calculate PCPM cell-based averages of each property. In this step, the averages of K_{th} property for cell n are calculated as

$$\overline{PK_n} = \sum_{j=1}^{L} PK_{m_j}/L \quad (3)$$

where the summation includes all L particles (m_1, m_2,..m_L) currently within cell n. L is the number of particles within that cell. If no particles are present in a particular cell, PCPM uses the values of $\overline{PK_n}$ from the previous time step.

Preprints (www.preprints.org) | NOT PEER-REVIEWED | Posted: 17 August 2018 doi:10.20944/preprints201808.0246.v2

5. Calculate the time evolution of the cell-based properties (and particle-based properties if necessary) using the process equation defined for that property. The process equations can incorporate terms which depend on either particle-based or cell-based properties, or both, i.e.

$$\overline{PK_n}(t+\Delta t) = FN(P1_M(t), P2_M(t), P3_M(t), \ldots \overline{P1_n}(t), \overline{P2_n}(t), \overline{P3_n}(t), \ldots) \quad (4)$$

Note that M indicates m_1, m_2,..m_L. The form of *FN* is completely general and depends on the problem being solved. For instance, in a NPZD model, the $Pi, (i = 1,2,3 \ldots$)would be N, P, Z, D, and water temperature, and the *FN* would be the process equations relating these properties. Since the cell-based averages have already been computed, the right-hand side of equation 4 is independent of the left-hand side, so the computation of the evolution equations can be carried out in parallel. This is another key design feature of PCPM allowing it to take full advantage of multiprocessing computer environments, both Symmetric Multi-Processing (SMP) and Massively Parallel Processing (MPP).

6. Redistribute cell-based properties to particles within each cell by replacing the particle-based property with a weighted average of the cell-based property. After the evolution equations have been carried out (Step 5), particles within an individual cell most likely carry a range of different values of the various properties, which vary around the new cell-based average computed in Step 5, $\overline{PK_n(t+\Delta t)}$. PCPM provides an optional step to reduce the variance of the new particle-based properties within each cell. This optional step is applied as a 'nudging' term, i.e.

$$PK_m(t+\Delta t) = (1-\alpha_i)PK_m(t) + \alpha_i \overline{PK_n(t+\Delta t)} \quad (5)$$

where $0<\alpha_i<1$ is the redistribution weight (i.e. nudging) factor. If α_i=0, no adjustment is carried out and particle-based property remain unchanged. If α_i=1, then all particles within a cell are assigned the cell-based average of that property. This step can be useful to smooth results when limited particle density results in excessive within-cell variability.

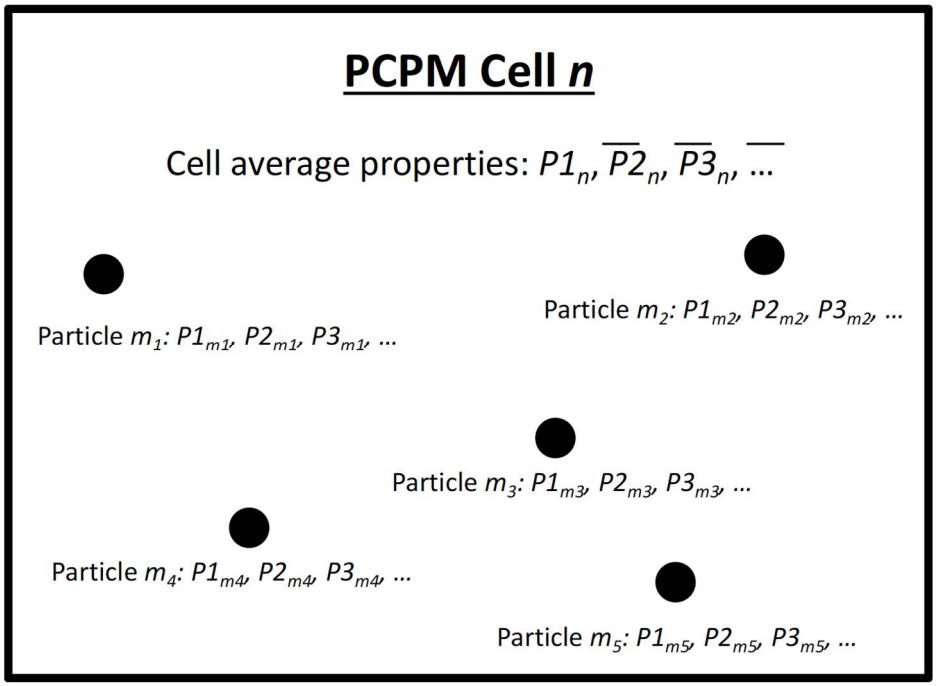

Figure 1. Conceptual representation of a PCPM computational cell n and particles (m_1, m_2, m_3, m_4, m_5...) within the cell n. PCPM cell-based average of each property ($\overline{P1_n}$, $\overline{P2_n}$, $\overline{P3_n}$,…) is determined by the property values carried by the particles that have entered in this cell. After time evolution of PCPM properties using process equations, the updated PCPM cell-based properties ($\overline{P1_n}$, $\overline{P2_n}$, $\overline{P3_n}$,…) are redistributed to particles with a weighted average. Then the particles move around carrying the updated properties to different PCPM computational cell in the next cycle.

Preprints (www.preprints.org) | NOT PEER-REVIEWED | Posted: 17 August 2018 doi:10.20944/preprints201808.0246.v2

3. Results of Idealized Cases

3.1. Advection-diffusion plume

In PCPM, diffusion is provided mainly by particle trajectories, although the cell-based averaging of particle properties and the (optional) redistribution of cell-based properties to particles within the cell can also act as diffusive terms. To demonstrate the effect of particle trajectory diffusion on particle properties, we constructed a 500 m wide x 2000 m long channel divided into 10 m square cells (Fig. 2). Particles were introduced at random locations along the center 400 m section of the left edge of the channel at the rate of 100/sec. The particles were assigned an along-channel velocity of 2 m/sec. Horizontal diffusion was added using a random-walk perturbation to the particle trajectories of $2r\sqrt{2k_h\Delta t}$ in both cross-channel and long-channel directions. Here, r is a uniformly distributed random number in the range [-1,1], k_h is the horizontal diffusion coefficient (10 m²/sec in this experiment), and Δt is the time step for the particle trajectory calculation (1 sec).

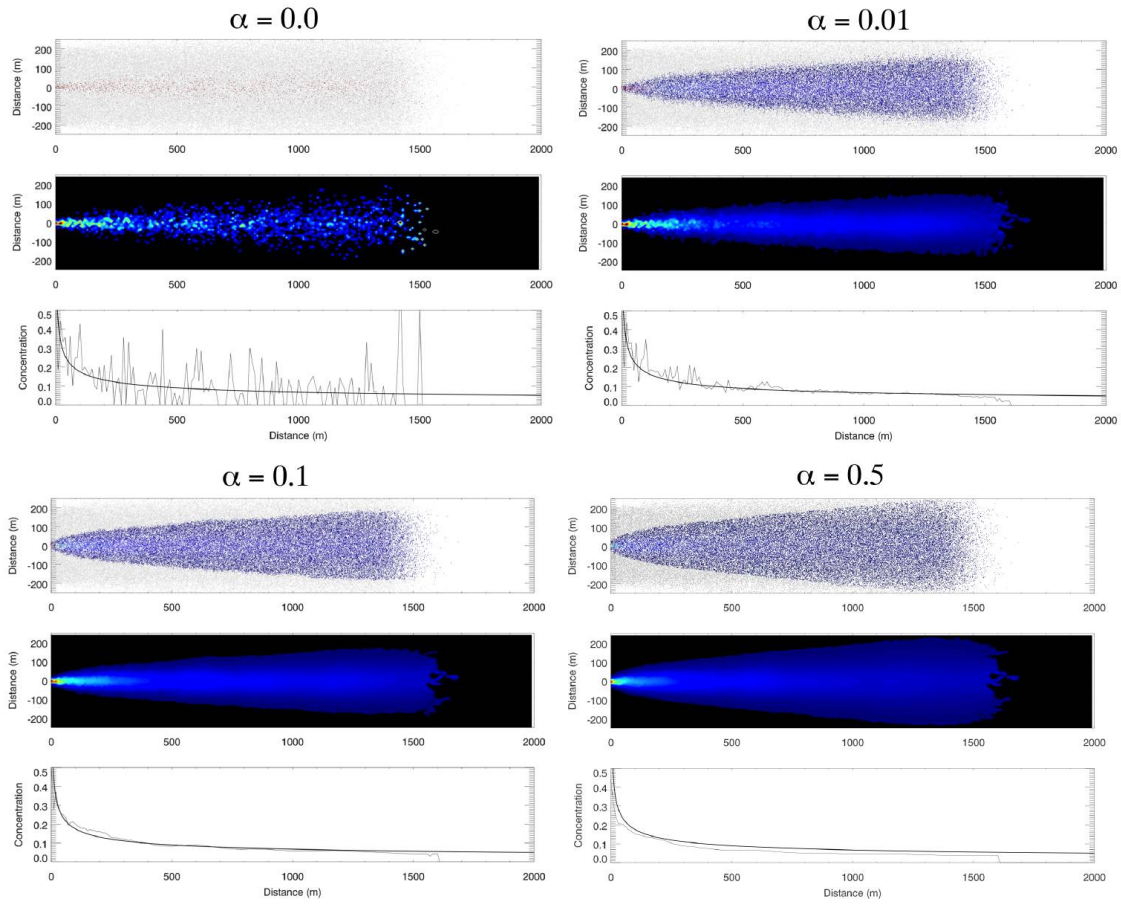

Figure 2. PCPM simulation of concentration plume in an idealized channel with four different values of the cell-based redistribution weight parameter (α = 0, 0.01, 0.1, 0.5). There are three panels for each value of α. The top panel shows the locations of particles after 720 time steps (12 minutes). The second panel shows the average concentration in each 10 m square cell with the same blue to red scale as the top panel, except cells with C = 0 are black. The third panel compares concentration along the centerline of the plume from the second panel to the analytical solution for a diffusive plume.

In this example, PCPM particles carry only one property, concentration (P1=C), and there is no time evolution equation (step 5, above). The purpose of this example is to illustrate how PCPM simulates horizontal diffusion through a combination of the particle trajectories and the cell-based averaging in step 6. To simulate a concentration plume, particles introduced in the center of the left wall (-50 m < y < 50 m) are assigned the initial condition C = 1. Particles entering the channel outside

Preprints (www.preprints.org) | NOT PEER-REVIEWED | Posted: 17 August 2018 doi:10.20944/preprints201808.0246.v2

this region have an initial condition of C = 0. To illustrate the effect of the cell-based averaging (step 6), we show results for four different values of the cell-based redistribution parameter (α = 0, 0.01, 0.1, 0.5) in Figure 2. In Figure 2, there are three panels for each value of α. The top panel shows the locations of particles after 720 time steps (12 minutes). The particles are colored using a blue-to-red scale for concentration values from 0 to 1. Particles with a concentration value of exactly 0 are colored light gray. The second panel shows the average concentration in each 10 m square cell with the same blue to red scale as the top panel, except cells with C = 0 are black. The third panel compares concentration along the centerline of the plume from the second panel to the analytical solution for a diffusive plume [9,10], i.e.,

$$C(x) = \mathrm{erf}([\tfrac{2}{3}([1.4x + 1]^{0.833} - 1)]^{-0.5}) \quad (6)$$

where $C(x)$ is the centerline concentration x meter away from the channel entrance. In the case α = 0, there is no cell-based redistribution of properties, so all particles retain their initial concentration values of either C=0 (light gray in panel 1) or C=1 (red in panel 1). As seen in the second and third panels, the random-walk diffusion in the particle trajectories does provide a rough approximation to the analytical solution by mixing of C=0 and C=1 particles in PCPM cells. Of course increasing the number of particles in the simulation would provide a more accurate approximation, but would also increase the computational load. Setting the cell-based redistribution parameter to even the small value of α = 0.01 provides a significant improvement in the solution with the same number of particles, particularly for x > 500 m. Now particles can have any value of C between 0 and 1. Increasing the redistribution parameter to α = 0.1 further improves the solution for x < 500 m. Further increasing α to 0.5 does not significantly improve the solution in comparison to α = 0.1.

3.2. Vertical settling

Since this implementation of PCPM does not allow the properties carried by the particles to influence particle trajectories, the question arises of how to simulate the vertical transport of a property when the vertical transport depends on the property itself, such as sediment settling or biologically generated buoyancy. In PCPM, the answer is simply to solve the vertical transport at the PCPM cell-based Eulerian framework in step 5 as a traditional cell-based method. Interaction of particle properties with adjacent cell averages is technically not allowed in the basic PCPM framework, but an exception is made in this case. The vertical advection-diffusion equation for sediment concentration is shown below

$$\frac{\partial C}{\partial t} = w_s \frac{\partial C}{\partial z} + k_z \frac{\partial^2 C}{\partial z^2} \quad (7)$$

where w_s is the bulk settling velocity of the suspended material and k_z is the vertical diffusion coefficient.

Since vertical diffusion is already included in the particle trajectories, PCPM only needs to consider the first term on the right-hand side of (7) to account for the additional vertical transport that depends on the property itself. To implement this term in PCPM, the process equation for a particle carrying a property C_m in vertical cell k looks like

$$C_m(t + \Delta t) = C_m(t) + w_s \Delta t\left(\overline{C_{k-1}(t)} - \overline{C_k(t)}\right)\Delta z + (other\ process\ terms) \quad (8)$$

where $\overline{C_k(t)}$ is the average concentration in vertical cell k, $\overline{C_{k-1}(t)}$ is the average concentration in the next higher vertical cell, and Δz is the spacing between the centers of the cells. For particles in the top cell (k=0), we set

$$C_m(t + \Delta t) = C_m(t) - w_s \Delta t \overline{C_0(t)} \Delta z + (other\ process\ terms) \quad (9)$$

and for particles in the bottom cell (k=$kmax$), we set

$$C_m(t + \Delta t) = C_m(t) - w_s \Delta t \overline{C_{kmax}(t)} \Delta z + (other\ process\ terms) \quad (10)$$

Preprints (www.preprints.org) | NOT PEER-REVIEWED | Posted: 17 August 2018 doi:10.20944/preprints201808.0246.v2

As a test case, we examine the vertical setting in a one-dimensional water column of depth d with particles moving vertically only through vertical diffusion. Particles are initially distributed randomly in the column and then move with a random walk velocity of $2r\sqrt{2k_z\Delta t}$ where r is a uniformly distributed random number in the range [-1,1] and k_z is the vertical diffusion coefficient. Particles are not allowed to cross the surface or bottom boundaries. Thus, in this experiment, the number of particles is constant and are always approximately uniformly distributed in the vertical due to vertical mixing.

For the experiment, we set $C = 1$ as the bottom boundary condition by assigning this value at the beginning of each time step to all particles in the lower half of the bottom cell. The initial condition in other cells is $C = 0$. For the test case, we set the number of particles to 1000, $d = 20$ m, $k_z = 10^{-4}$ m^{2}s^{-1}, and the redistribution parameter = 0.1. Three runs were made with 5, 10, and 20 vertical cells respectively. PCPM is integrated in time with $\Delta t = 1$ hr. The results at the end of 5,000 time steps are shown in Figure 3. In Figure 3, the dots represent the locations of the particles on the vertical axis and the value of concentration they are carrying on the horizontal axis. The thin line is the cell average concentration. The thick line is the analytical solution,

$$C = e^{\frac{-w_s}{k_z}z} \tag{11}$$

As shown in Figure 3, the model properly simulates the change in concentration due to vertical settling and mixing while allows the particles to remain approximately uniformly distributed in the vertical. The simulation accuracy increases with increased resolution of vertical layers. The model result with 20 vertical layers shows a close agreement with the analytical solution. Specifically, Figure 4 shows the evolution in time of the root mean square difference (RMSD) between the cell averages and the analytical solution for the three cases. While the RMSD in the simulation with 5 layers remains above 0.2 (the magnitude of initial error) over the entire simulation, the RMSD decrease quickly to 0.02 after 500 time steps and stay stable at such level when vertical resolution increases to 20 layers.

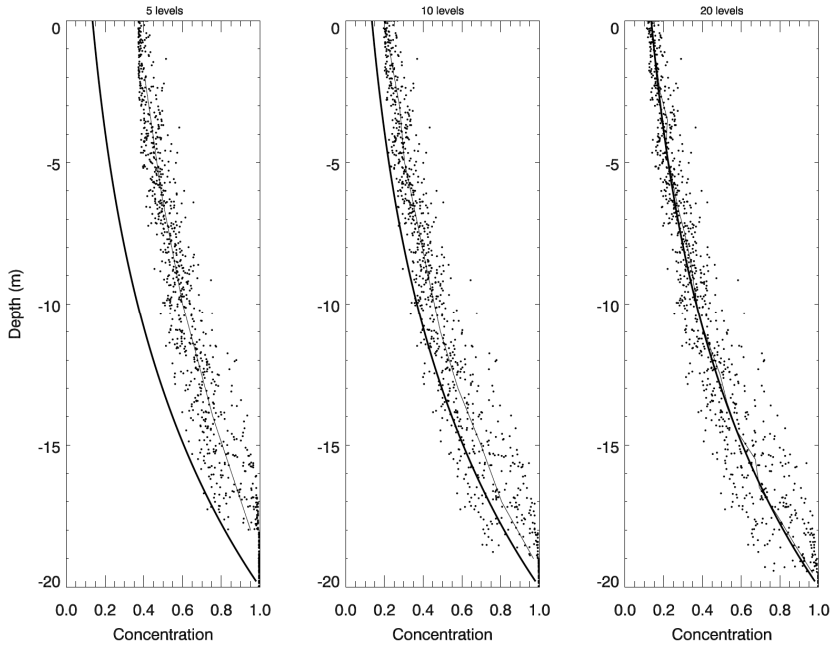

Figure 3. The PCPM simulation of vertical settling in comparison to the analytical solution at the end of 5,000 time steps. Three runs were made with 5, 10, and 20 vertical cells, respectively. The dots represent the locations of the particles on the vertical axis with their respective concentration on the horizontal axis. The thin line represents the cell average concentration and the thick line represents the analytical solution.

Preprints (www.preprints.org) | NOT PEER-REVIEWED | Posted: 17 August 2018 doi:10.20944/preprints201808.0246.v2

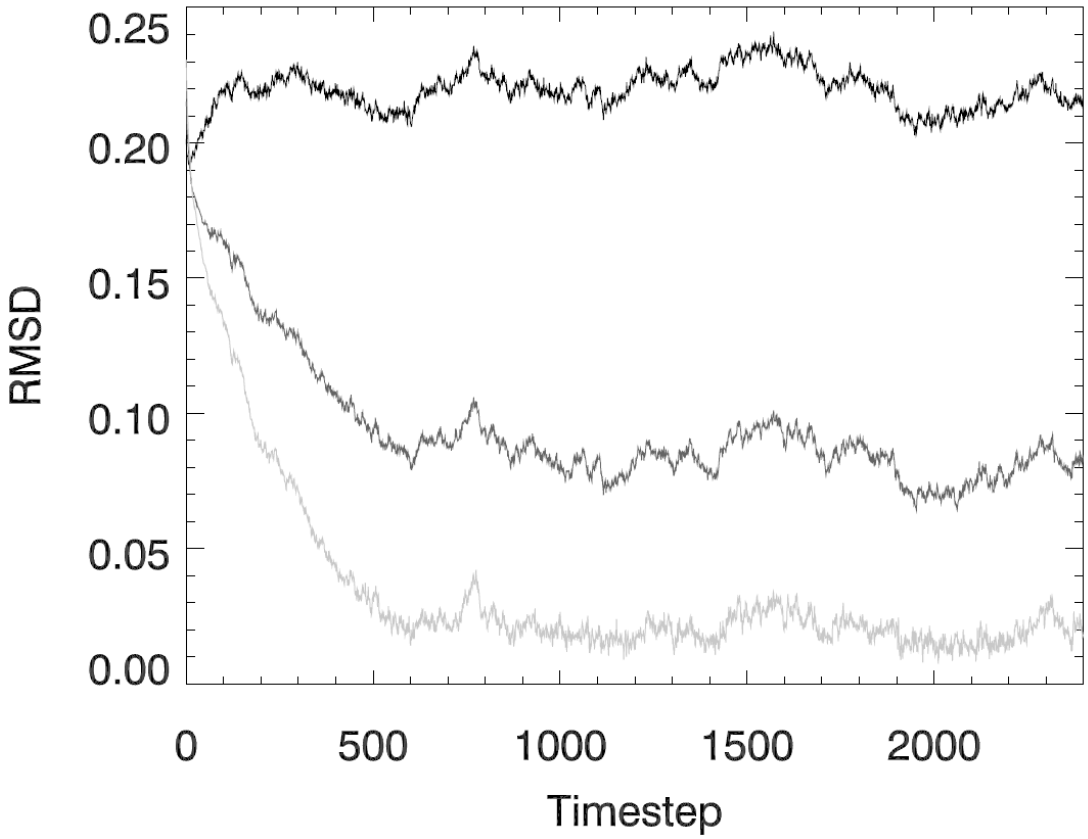

Figure 4. The time evolution of the root mean square difference (RMSD) between the cell averages and the analytical solution for the three cases presented in the Figure 3 (dark line for 5 cells, medium line for 10 cells, and light line for 20 cells).

4. Application to Sandusky Bay

To illustrate more clearly the type of application envisioned for PCPM, we constructed and applied a rudimentary biophysical model to an actual aquatic system, Sandusky Bay. Since the mid-1990s, harmful algal blooms (HABs) have become the new norm for summer months in the Lake Erie ecosystem [11]. Harmful algal blooms occur in the system when cyanobacteria are provided the right temperature, light, and nutrient conditions to proliferate. When these blooms transpire, they have many adverse impacts. At the local ecosystem level, HABs result in depleted dissolved oxygen levels below the lake's surface threatening the survival of organisms living below the surface. Additionally, some cyanobacteria species produce a toxin, such as microcystin, which affects the nervous system, liver, and kidney further impeding aquatic organisms and humans.

Situated on Lake Erie's southwestern coast is the focus of this study, Sandusky Bay (Fig. 5). Sandusky Bay borders Ohio's Ottawa, Erie, and Sandusky counties. Each of which relies heavily on Sandusky Bay. From a physical aspect, Sandusky Bay is relatively shallow bay with an average depth of roughly 2.6 meters as well as occupying a relatively small area [12]. The primary draining watershed to Sandusky Bay is originates from the Sandusky River on the west end of the bay. The Sandusky River drains a 1,420 square mile area; of which, over 80% is dedicated to agricultural production [11]. This largely agricultural watershed leads to high nitrogen and phosphorus entering Sandusky Bay. Combining these high nutrient loads with the physical aspects leads to very high concentrations of nitrogen and phosphorus within Sandusky Bay, thus resulting in these cyanobacteria blooms (Planktothrix *agardhii*) [12,13].

Preprints (www.preprints.org) | NOT PEER-REVIEWED | Posted: 17 August 2018 doi:10.20944/preprints201808.0246.v2

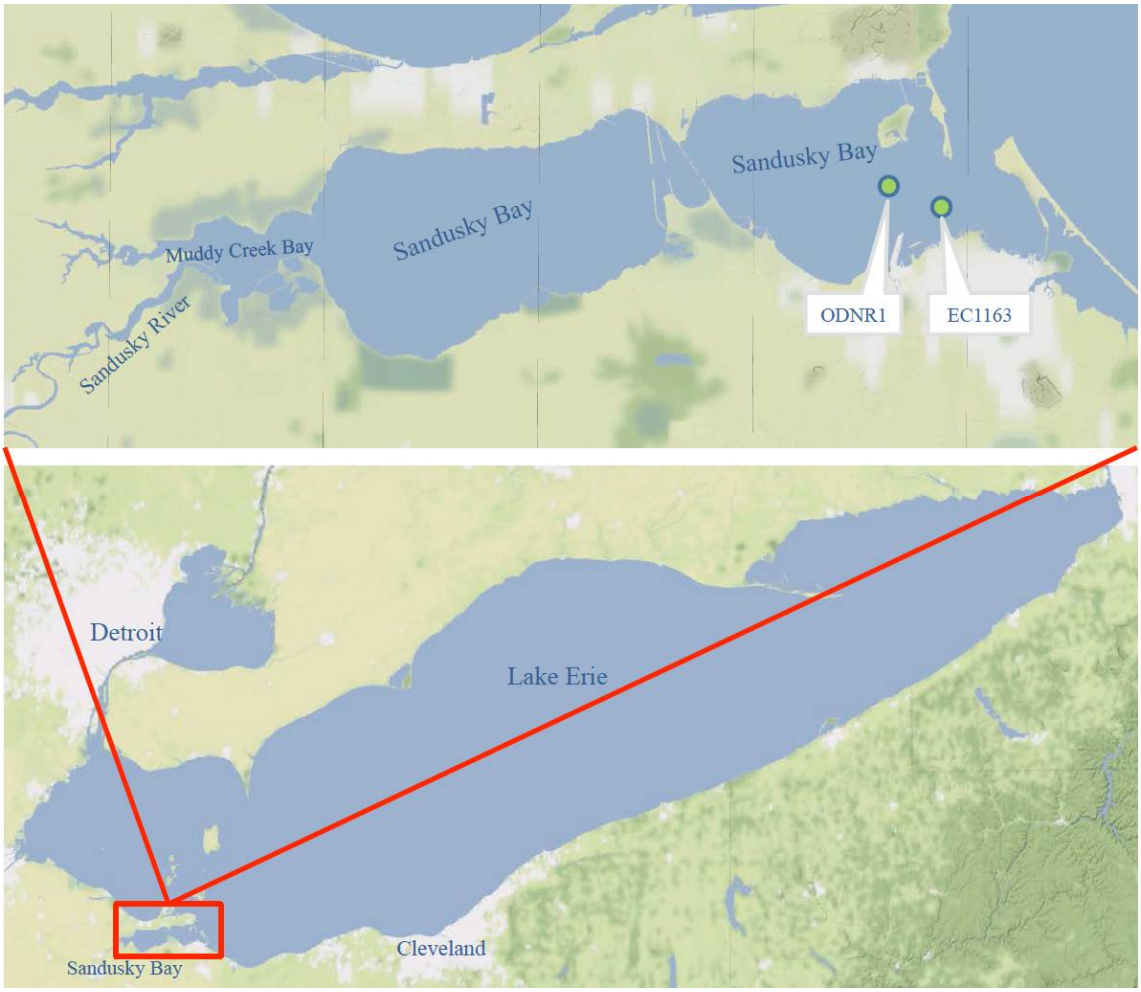

Figure 5. Sandusky Bay is situated on Lake Erie's southwest coast occupying a small portion of the Great Lake's coastline. Sandusky Bay is relatively shallow bay with an average depth of ~2.6 meters. The primary draining watershed to Sandusky Bay originates from the Sandusky River on the west end of the bay. Sampling stations ODNR1 and EC1163 are denoted with green dots.

In this study, the intent of the work is to test the PCPM feasibility for biological-physical coupled model by implementing it in relation to HABs in Sandusky Bay. The physical model utilizes the 3-D Finite Volume Community Ocean Model (FVCOM) based on an unstructured grid. The biological model is a 1-D NPZD model.

4.1. Observational Data

To aid in model development, several datasets are gathered from literature as well as data acquisition organizations. Sandusky river daily discharge and nitrogen concentration are available from National Center for Water Quality Research (https://ncwqr.org/monitoring/data/). Nitrogen, Chlorophyll concentration, and in-situ temperature data are available from two observational sites (ODNR1 and EC1163) in the eastern bay from May – October 2015, sampled by Bowling Green State University [13].

4.2. Hydrodynamic Model

The hydrodynamic model used in this study is FVCOM (Finite Volume Community Ocean Model) [14]. FVCOM is an unstructured-grid, finite-volume, three-dimensional (3-D) primitive equation ocean model with a generalized, terrain-following coordinate system in the vertical and a triangular mesh in the horizontal. The unstructured grid can be designed to provide a customized variable resolution to both coastline and bathymetry. With the merits of ideal geometric fitting and

 doi:10.20944/preprints201808.0246.v2

local refinement of mesh resolution, FVCOM has been used in numerous applications to estuaries, coastal oceans, and the Great Lakes [16-20]. These characteristics make the model well suited for the study of Sandusky Bay.

Although this study focuses on Sandusky Bay, FVCOM is configured to simulate physical dynamics for all of Lake Erie, thus providing reliable representation of large scale background circulation and the role of remote forcing impacting the water movement in the bay through the opening; additionally, this configuration avoids the impact of setting an artificial numerical boundary condition for our target region. The hydrodynamic model is well-calibrated for the Lake Erie, based on the next-generation NOAA Lake Erie Operational Forecast System [LEOFS; see Kelley et al., [21] for detailed model validation], a real-time nowcast and forecast model that is built on the FVCOM. In the upgraded NOAA operational model for Lake Erie [21], the FVCOM model is developed with horizontal resolution ranging from 100 to 2500 meters, and 21 uniform vertical sigma (terrain-following) layers for Lake Erie. The advantage of our model setting is that model resolution varies from 100-2500 m (coarse) in the open lake to 10-50 m (fine) in Sandusky Bay, affording a high degree of resolution across the 20 km x 3 km study site and adequately resolving the geographic complexity and coastal hydrodynamic conditions of that system (Figure 6). The model configuration yields a total of 73,000 grid elements (cells) in the horizontal plane with 50,000 of them resolving the bay.

Figure 6. FVCOM model mesh for Lake Erie (upper panel) and linked with a high-resolution mesh for Sandusky Bay (lower panel). Only a portion of the Sandusky Bay mesh is displayed for a clear representation of the mesh's resolution.

Preprints (www.preprints.org) | NOT PEER-REVIEWED | Posted: 17 August 2018 doi:10.20944/preprints201808.0246.v2

4.3. Biological Model

The biological model used in this work is a general 1-D NPZD model. The governing equations for the model framework are based on Luo et al. [22]. Figure 7 displays the interactions among state variables in the NPZD model.

$$\frac{dN}{dt} = -P(uptake) + Z(respiration) + P(respiration) + D(remineralization) + N(mixing)$$

$$\frac{dP}{dt} = P(uptake) - P(respiration) - P(mortality) - ZP(grazing) + P(mixing)$$

$$\frac{dZ}{dt} = ZP(grazing) + ZD(grazing) - Z(respiration) - Z(mortality) + Z(mixing)$$

$$\frac{dD}{dt} = P(mortality) + Z(mortality) - ZD(grazing) - D(remineralization) + D(mixing)$$

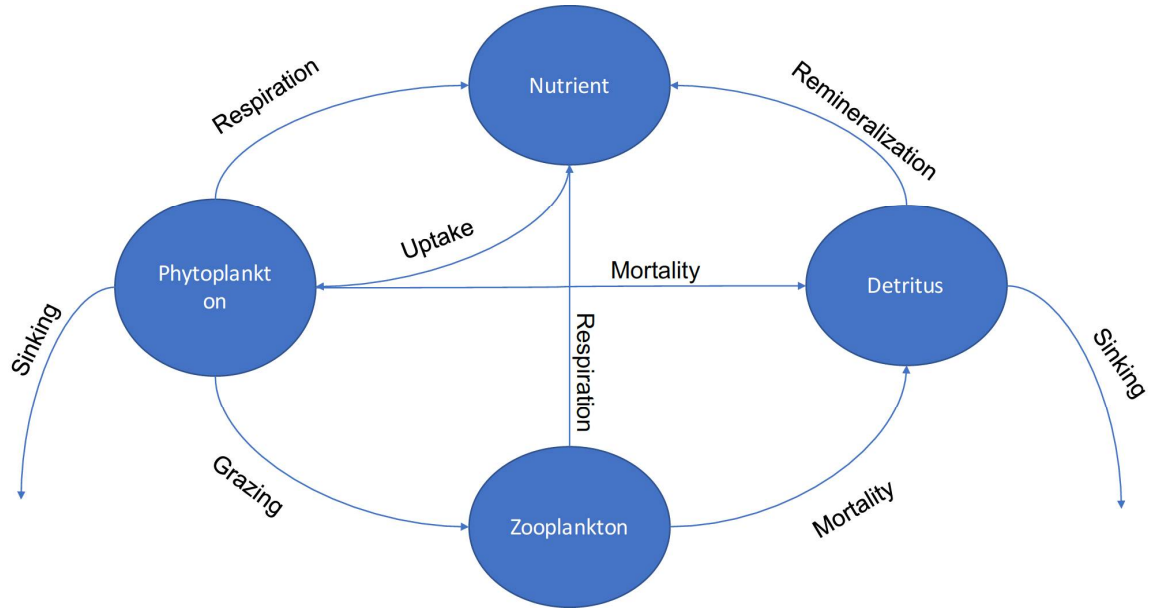

Fig. 7. A schematic representation of the NPZD model.

Several equations in the governing equations are modified for this study based on literature review. The light-limited, nutrient-limited, and temperature-limited functions $(f(I), f(N), f(T)$, respectively, that contribute to the $P(uptake)$ are taken from Platt et al. [23] and Nicklisch et al. [24]. Also, the light attenuation functions are adjusted to Rowe et al. [25].

$$f(I) = (1 - e^{-\frac{\alpha_I I}{\mu_{max}}})e^{-\frac{\beta_I I}{\mu_{max}}} \quad (12)$$

$$f(N) = \frac{N - N_0}{K_s + N - N_0} \quad (13)$$

$$f(T) = \exp(-2.3(\frac{T_{opt} - T}{T_{opt} - T_{min}})^2) \quad (14)$$

$$I = I_0 \exp(-k_d h) \quad (15)$$

where α_I, β_I are the initial linear slope at low irradiance and the negative slope at the high irradiance that characterizes photoinhibition [26], μ_{max} is the maximum potential growth rate, and I is the light intensity. The nutrient threshold N_0 represents the pool of nutrient that was assumed to be biologically unavailable. T_{opt} and T_{min} are the optimal growth temperature and minimal growth temperature, respectively. k_d is the light attenuation coefficient that accounts for the impact of

Preprints (www.preprints.org) | NOT PEER-REVIEWED | Posted: 17 August 2018 doi:10.20944/preprints201808.0246.v2

water turbidity, phytoplankton, and detritus on the light attenuation. Model parameterization is based on literature review [22,24-26] and subjective tuning for the Sandusky Bay simulation.

To ensure validity of the 1-D NPZD biological model, several scenarios from Edwards et al. [27] are reproduced with the same model configuration. As an example, Figure 8 demonstrates the linear stability of a vertically-distributed, NPZ ecosystem model and the impact of vertical mixing on biological dynamics. The nutrient-phytoplankton-zooplankton concentrations in terms of nitrogen (μmol N L^{-1}) at different depths are displayed in the water column. In the surface waters, it reaches equilibrium values. Notice in the second panel (depth = 25.5 m), oscillations develop in the curves indicating the model's instability below this depth. Under linear stability analysis, this incidence can be discerned from the fact that the eigenvalues have a real part [27]. However, at unstable mid-depths the fields return to equilibrium, as a damped oscillator due to vertical mixing, consistent with complex eigenvalues from linear stability analysis [27].

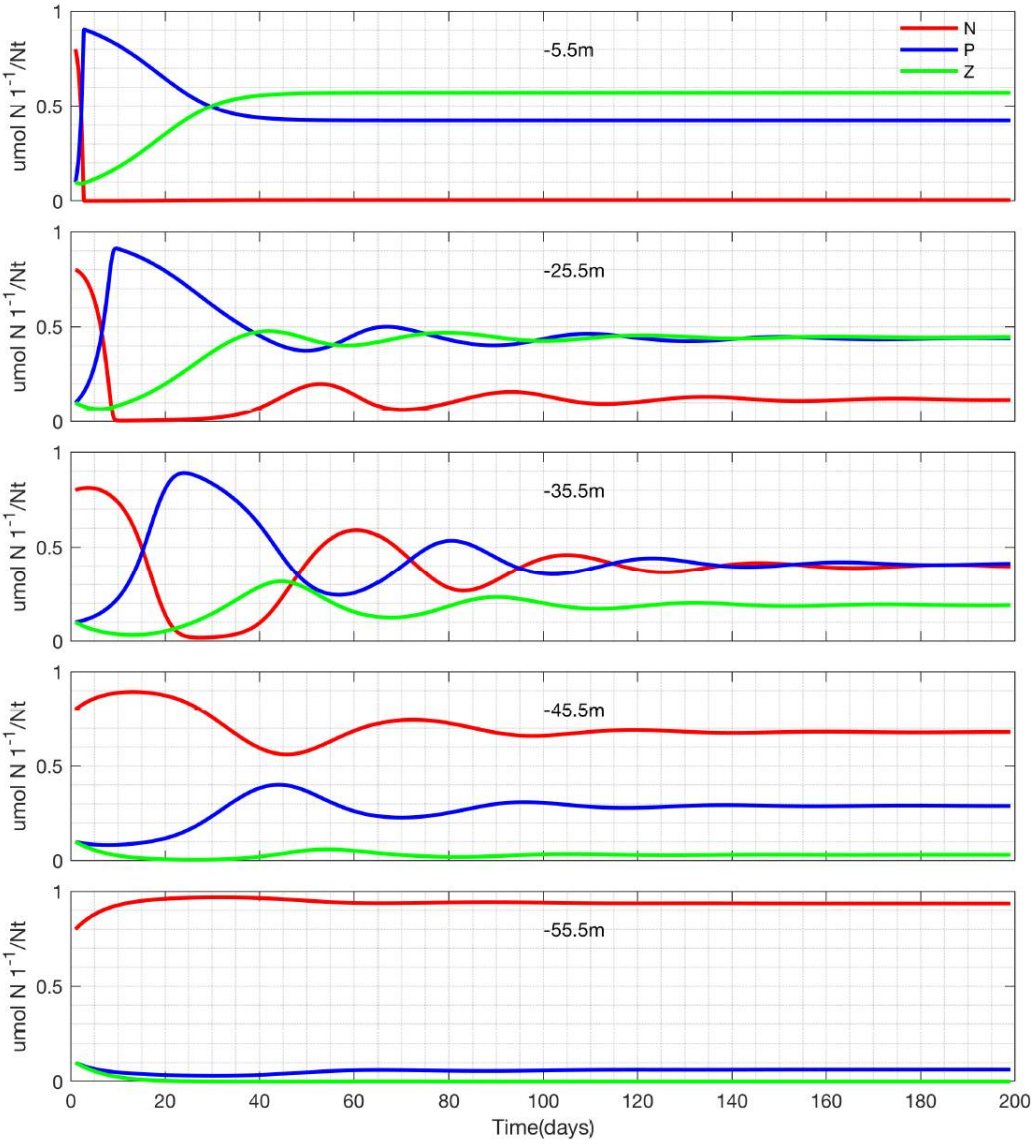

Figure 8. Reproduced scenarios using our NPZD model from Figure 6 in Edwards et al. [27] as a biological model verification, in which detritus is not considered. Time series solution of the diffusive NPZ model at depths (a) 5 m, (b) 25 m, (c) 35 m, (d) 45 m, and (e) 55 m. Notice that in the water layer below 25.5 m, there are damped oscillations over time, consistent with the linear stability analysis showing complex eigenvalues with negative real parts below 25.5m. See detailed discussion in the linear stability analysis in Edwards et al. [27].

Preprints (www.preprints.org) | NOT PEER-REVIEWED | Posted: 17 August 2018 doi:10.20944/preprints201808.0246.v2

4.4 Results

Before examining the impact of physical transport on the biological dynamics, we first validate the representation of advection-diffusion in PCPM. The river plume is simulated using the conventional soluble-tracer model based on Equation 1 and PCPM model for plume modeling (Fig. 9). It is clear that the plumes simulated using the two methods show a very similar pattern, indicating the validity of the PCPM. Upon closer review, the plume simulated with soluble-tracer model shows a smoother evolution near the plume front, and a better representation of plume in Muddy Creek Bay in comparison to the PCPM. This indicates denser particles release may be needed in the mouth of the Sandusky River. Nonetheless, the attractiveness of PCPM is its computation efficiency; it runs ~100 times faster than the soluble-tracer model which will be discussed in detail in the following section.

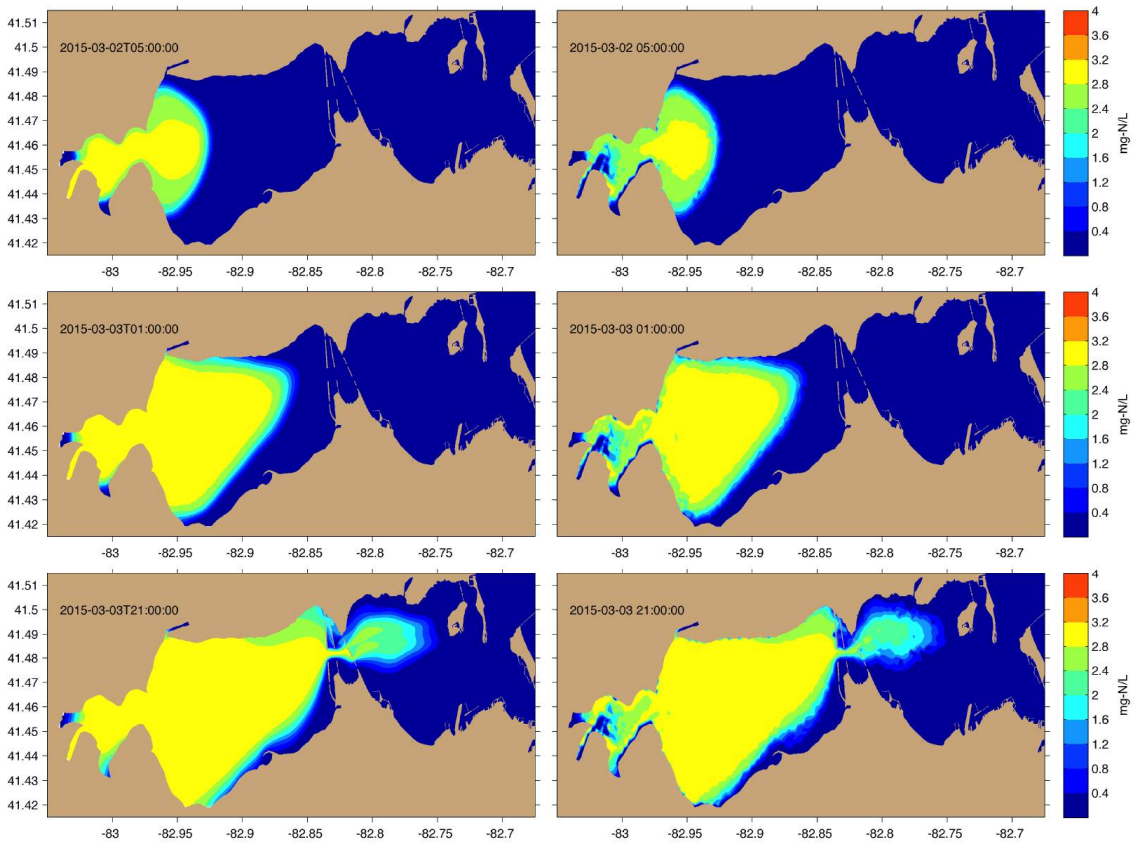

Figure 9. River plumes simulated with conventional soluble-tracer model (left panels) and PCPM model (right panels). The color scale represents the nitrogen concentration.

Using the PCPM-NPZD model, the importance of physical transport is demonstrated by comparing model results between the NPZD standalone simulation and PCPM-NPZD simulation. The comparison of model results is presented in Figure 10. The simulation using NPZD standalone model without resolving the transport processes shows a large discrepancy from observational data (Fig. 10, upper panels). The model completely fails to capture both the timing and magnitude of the blooms. On the other hand, after the impact of advective processes is resolved using PCPM, the model accurately depicts the magnitude of the chlorophyll peak in mid-August. Although further development of the NPZD is certainly necessary to resolve the onset and variability of the algal blooms, it is beyond the scope of this work, which focuses on demonstrating the feasibility of linking hydrodynamic effects and biological processes through the PCPM in a Lagrangian/Eulerian framework. The further development of the biological model and its application to the mechanisms study for the HABs in Sandusky Bay will be presented in a companying paper.

Preprints (www.preprints.org) | NOT PEER-REVIEWED | Posted: 17 August 2018 doi:10.20944/preprints201808.0246.v2

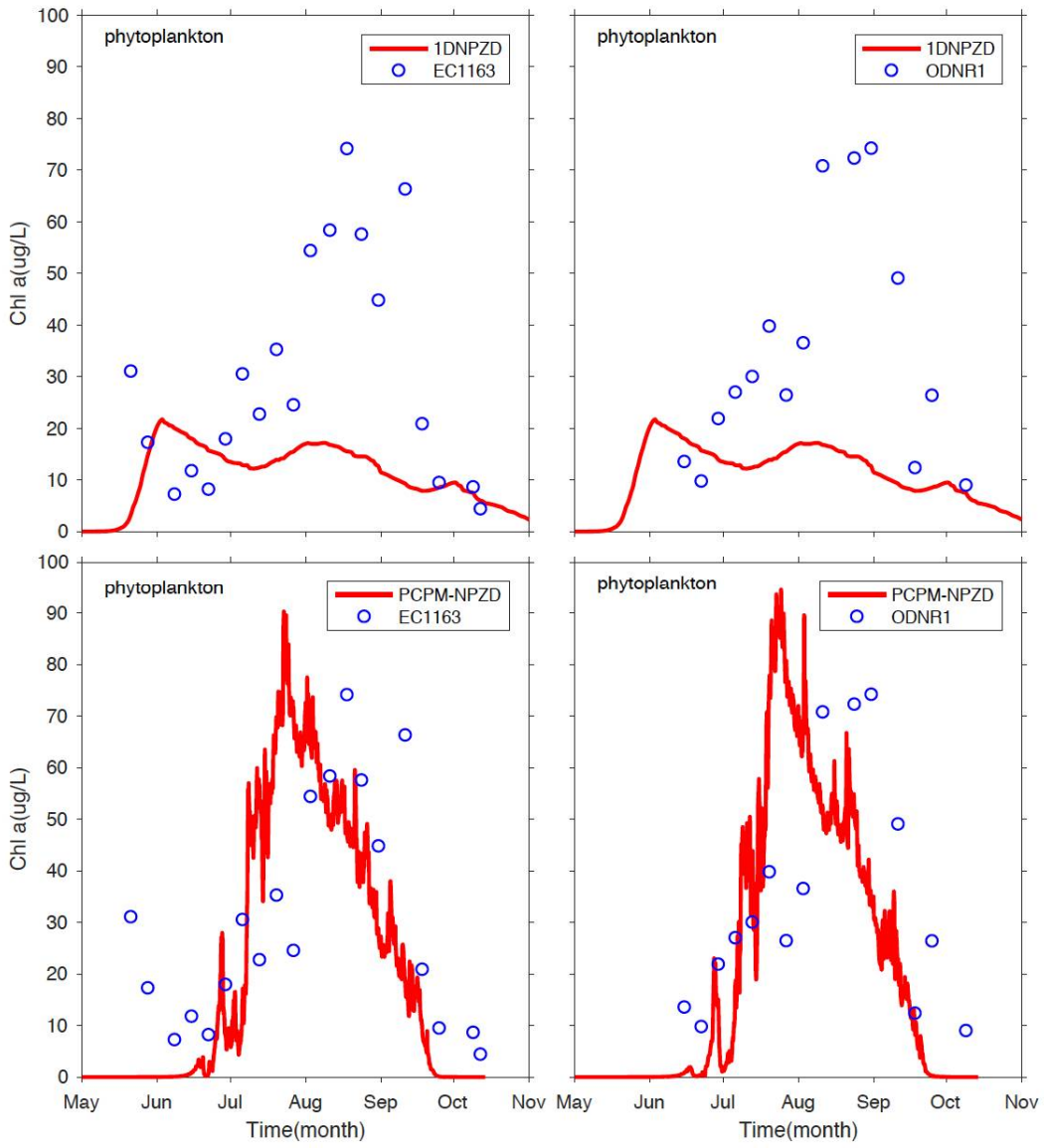

Figure 10. Observed (blue dots) and model simulated (red lines) Chlorophyll concentration at the sampling stations EC1163 and ODNR1. The upper panels are results from the standalone 1-D NPZD model simulation; the lower panel are the results from the coupled PCPM-NPZD model simulation.

5. Summary and Conclusions

In this paper, we describe a novel method by integrating a property-carrying particle model (PCPM) and an Eulerian concentration biological model for ecosystem modeling. The model is tested in idealized cases and its utility is demonstrated in a practical application to Sandusky Bay. The novelty of this new technique lies in its integration of hydrodynamic effects via the property-carrying particle tracking model and Eulerian grid-based biological modeling approach. Overall, there are several advantages of the PCPM over traditional Eulerian-based tracer approaches. The PCPM is simpler to implement and more efficient as it does not need to solve the advection-diffusion equation. Instead, the PCPM uses pre-computed particle trajectories to resolve the hydrodynamic condition based on currents from a hydrodynamic model. This means that the hydrodynamic model only needs to be run once giving one the ability to run different biological scenarios for the same physical characteristics; ultimately saving significant computational time.

For example, 1-year hydrodynamic simulation with the particle tracking model in Sandusky Bay case takes 5 day to complete using 64 CPUs. Once the hydrodynamic simulation is done, the PCPM can complete its 1-year river plume simulation using the particle trajectories as input within 10

minutes using a single CPU while it takes 12 hours for soluble-tracer model to complete the same simulation using 32 CPUs. In the PCPM framework, the hydrodynamics and associated water transport and mixing represented by particle trajectories are "reserved" and not affected by biochemical properties. In other words, it only takes another 10 minutes to run the PCPM for a different set of parameters and property configurations. This is extremely useful during the model calibration and or ensemble simulations. Such a high level of efficiency is not available from tracer-based models because one will have to re-run the soluble-tracer model for any change in parameter configuration or estimation of different property concentration. In addition, the PCPM is capable of providing comparable simulation results to the soluble-tracer model, although the global and local mass conservation is not strictly preserved with finite particles. Above all, it is the PCPM's computational efficiency and coupling flexibility which makes it an attractive alternative method to the traditional approach.

Author Contributions: Conceptualization, Pengfei Xue and David Schwab; Formal analysis, Xing Zhou, Chenfu Huang and Xinyu Ye; Project administration, Pengfei Xue; Validation, Xing Zhou; Visualization, Xing Zhou, Chenfu Huang and Xinyu Ye; Writing – original draft, Pengfei Xue and David Schwab; Writing – review & editing, Pengfei Xue, David Schwab and Ryan Kibler.

Funding: This work is partly supported by the National Oceanic and Atmospheric Administration, grant# NA17NOS4780186.

Acknowledgments: This is the contribution XX of the Great Lakes Research Center at Michigan Technological University.

Conflicts of Interest: The authors declare no conflict of interest.

References

1. Chen, C., Xu, Q., Houghton, R., & Beardsley, R. C. (2008). A model-dye comparison experiment in the tidal mixing front zone on the southern flank of Georges Bank. Journal of Geophysical Research: Oceans, 113(C2).
2. Xue, P., Chen, C., Ding, P., Beardsley, R. C., Lin, H., Ge, J., & Kong, Y. (2009). Saltwater intrusion into the Changjiang River: A model-guided mechanism study. Journal of Geophysical Research: Oceans, 114(C2).
3. Feddersen, F., Olabarrieta, M., Guza, R. T., Winters, D., Raubenheimer, B., & Elgar, S. (2016). Observations and modeling of a tidal inlet dye tracer plume. Journal of Geophysical Research: Oceans, 121(10), 7819-7844.
4. Jiang, L., & Xia, M. (2018). Modeling investigation of the nutrient and phytoplankton variability in the Chesapeake Bay outflow plume. Progress in Oceanography, 162, 290-302.
5. Harlow, F.H. (1964). The Particle-in-Cell Computing Method for Fluid Dynamics. Methods in Computational Physics, 3, 319-343.
6. Harlow, F.H. (1988). PlC and Its Progeny. Computer Physics Communications, 48, 1—10.
7. Hockney, R. W., and Eastwood, J. W. (1981). Computer Simulation Using Particles. McGraw-Hill, New York.
8. Grigoryev, Y.N., V.A. Vshivkov, and M.P. Fedoruk (2002). Numerical "Particle-in-Cell" Methods: Theory and Applications. De Gruyter VSP, Utrecht, Boston, 249pp.
9. Stacey, M.T., E.A. Cowen, T.M. Powell, E. Dobbins, S.G. Monismith, and J.R. Koseff (2000). Plume dispersion in a stratified, near-coastal flow: measurements and modeling. Continental Shelf Research, 20, 637-663.
10. Kim, T. and T. Khangaonkar (2012). An offline unstructured biogeochemical model (UBM) for complex estuarine and coastal environments. Environmental Modelining and Software, 31, 47-63.
11. U.S. EPA. (2017, Aug 10). *U.S. Action Plan for Lake Erie.* Retrieved from https://www.epa.gov/sites/production/files/2017/08/documents/us_dap_preliminary_draft_for_public_engagement_8-10-17.pdf

12. Davis, T. W., Bullerjahn, G. S., Tuttle, T., McKay, R. M., & Watson, S. B. (2015). Effects of increasing nitrogen and phosphorus concentrations on phytoplankton community growth and toxicity during Planktothrix blooms in Sandusky Bay, Lake Erie. *Environmental science & technology*, *49*(12), 7197-7207.
13. Salk, K. R., Bullerjahn, G. S., McKay, R. M. L., Chaffin, J. D., & Ostrom, N. E. (2018). Nitrogen cycling in Sandusky Bay, Lake Erie: oscillations between strong and weak export and implications for harmful algal blooms. *Biogeosciences*, *15*(9), 2891.
14. Chen, C., Huang, H., Beardsley, R. C., Liu, H., Xu, Q., & Cowles, G. (2007). A finite volume numerical approach for coastal ocean circulation studies: Comparisons with finite difference models. Journal of Geophysical Research: Oceans, 112(C3).
15. Yang, Z., Wang, T., & Copping, A. E. (2013). Modeling tidal stream energy extraction and its effects on transport processes in a tidal channel and bay system using a three-dimensional coastal ocean model. Renewable Energy, 50, 605-613.
16. Xue, P., Schwab, D. J., & Hu, S. (2015). An investigation of the thermal response to meteorological forcing in a hydrodynamic model of Lake Superior. Journal of Geophysical Research: Oceans, 120(7), 5233-5253.
17. Anderson, E. J., Bechle, A. J., Wu, C. H., Schwab, D. J., Mann, G. E., & Lombardy, K. A. (2015). Reconstruction of a meteotsunami in L ake E rie on 27 M ay 2012: Roles of atmospheric conditions on hydrodynamic response in enclosed basins. Journal of Geophysical Research: Oceans, 120(12), 8020-8038.
18. Xue, P., J. S. Pal, X. Ye, J. D. Lenters, C. Huang, and P. Y. Chu (2017), Improving the Simulation of Large Lakes in Regional Climate Modeling: Two-Way Lake–Atmosphere Coupling with a 3D Hydrodynamic Model of the Great Lakes, *J. Climate, 30*, 1605-1627.
19. Khangaonkar, T., Nugraha, A., Xu, W., Long, W., Bianucci, L., Ahmed, A., ... & Pelletier, G. (2018). Analysis of Hypoxia and Sensitivity to Nutrient Pollution in Salish Sea. Journal of Geophysical Research: Oceans.
20. Ye, X., E. J. Anderson, P. Y. Chu, C. Huang, and P. Xue (2018). Impact of water mixing and ice formation on deep, inland lake warming: a model-guided mechanism study. Limnology and Oceanography, (in revision)
21. Kelley, J. G. W., Y. Chen, E. J. Anderson, G. A. Lang, and J. Xu, 2018. Upgrade of NOS Lake Erie Operational Forecast System (LEOFS) To FVCOM: Model Development and Hindcast Skill Assessment. NOAA Technical Memorandum NOS CS 40, 92 pp.
22. Luo, L., Wang, J., Schwab, D. J., Vanderploeg, H., Leshkevich, G., Bai, X., ... & Wang, D. (2012). Simulating the 1998 spring bloom in Lake Michigan using a coupled physical-biological model. *Journal of Geophysical Research: Oceans*, *117*(C10).
23. Nicklisch, A., Shatwell, T., & Köhler, J. (2007). Analysis and modelling of the interactive effects of temperature and light on phytoplankton growth and relevance for the spring bloom. *Journal of Plankton Research*, *30*(1), 75-91.
24. Platt, T. G. C. L., Gallegos, C. L., & Harrison, W. G. (1980). Photoinhibition of photosynthesis in natural assemblages of marine phytoplankton.
25. Rowe, M. D., Anderson, E. J., Vanderploeg, H. A., Pothoven, S. A., Elgin, A. K., Wang, J., & Yousef, F. (2017). Influence of invasive quagga mussels, phosphorus loads, and climate on spatial and temporal patterns of productivity in Lake Michigan: A biophysical modeling study. *Limnology and Oceanography*, *62*(6), 2629-2649.
26. Fahnenstiel, G. L., Chandler, J. F., Carrick, H. J., & Scavia, D. (1989). Photosynthetic characteristics of phytoplankton communities in Lakes Huron and Michigan: PI parameters and end-products. *Journal of Great Lakes Research*, *15*(3), 394-407.
27. Edwards, C. A., Powell, T. A., & Batchelder, H. P. (2000). The stability of an NPZ model subject to realistic levels of vertical mixing. *Journal of Marine Research*, *58*(1), 37-60.